HHS Public Access

Author manuscript

Adv Funct Mater. Author manuscript; available in PMC 2021 November 11.

Published in final edited form as:

Adv Funct Mater. 2020 November 11; 30(46): . doi:10.1002/adfm.202004285.

Rapidly-customizable, scalable 3D-printed wireless optogenetic probes for versatile applications in neuroscience

Juhyun Lee[†],
School of Electrical Engineering, Korea Advanced Institute of Science and Technology (KAIST), Daejeon 34141, Republic of Korea

Kyle E. Parker[†],
Department of Pharmaceutical and Administrative Sciences, St. Louis College of Pharmacy; Center for Clinical Pharmacology, St. Louis College of Pharmacy and Washington University School of Medicine; Department of Anesthesiology, Washington University Pain Center, Department of Psychiatry, Washington University in St. Louis, St. Louis, Missouri 63130, USA

Chinatsu Kawakami[†],
Department of Electrical and Electronic Information Engineering, Toyohashi University of Technology, Toyohashi 441-8580, Japan

Jenny R. Kim[†],
Department of Pharmaceutical and Administrative Sciences, St. Louis College of Pharmacy; Center for Clinical Pharmacology, St. Louis College of Pharmacy and Washington University School of Medicine; Department of Anesthesiology, Washington University Pain Center, Department of Psychiatry, Washington University in St. Louis, St. Louis, Missouri 63130, USA

Raza Qazi,
School of Electrical Engineering, Korea Advanced Institute of Science and Technology (KAIST), Daejeon 34141, Republic of Korea

Junwoo Yea,
Department of Robotics Engineering, Daegu Gyeongbuk Institute of Science and Technology (DGIST), Daegu 42988, Republic of Korea

Shun Zhang,
Department of Mechanical Engineering, University of Colorado Boulder, Boulder, Colorado 80309, USA

Choong Yeon Kim,
School of Electrical Engineering, Korea Advanced Institute of Science and Technology (KAIST), Daejeon 34141, Republic of Korea

John Bilbily,

[*]To whom correspondence should be addressed. jordangmccall@wustl.edu (J.G.M.); jjeong1@kaist.ac.kr (J.-W.J.).
[†]These authors contributed equally to this work.

Supporting Information
Supporting Information is available from the Wiley Online Library or from the author.

Department of Pharmaceutical and Administrative Sciences, St. Louis College of Pharmacy; Center for Clinical Pharmacology, St. Louis College of Pharmacy and Washington University School of Medicine; Department of Anesthesiology, Washington University Pain Center, Department of Psychiatry, Washington University in St. Louis, St. Louis, Missouri 63130, USA

Jianliang Xiao,
Department of Mechanical Engineering, University of Colorado Boulder, Boulder, Colorado 80309, USA

Kyung-In Jang,
Department of Robotics Engineering, Daegu Gyeongbuk Institute of Science and Technology (DGIST), Daegu 42988, Republic of Korea

Jordan G. McCall*,
Department of Pharmaceutical and Administrative Sciences, St. Louis College of Pharmacy; Center for Clinical Pharmacology, St. Louis College of Pharmacy and Washington University School of Medicine; Department of Anesthesiology, Washington University Pain Center, Department of Psychiatry, Washington University in St. Louis, St. Louis, Missouri 63130, USA

Jae-Woong Jeong*
School of Electrical Engineering, Korea Advanced Institute of Science and Technology (KAIST), Daejeon 34141, Republic of Korea

Abstract

Optogenetics is an advanced neuroscience technique that enables the dissection of neural circuitry with high spatiotemporal precision. Recent advances in materials and microfabrication techniques have enabled minimally invasive and biocompatible optical neural probes, thereby facilitating *in vivo* optogenetic research. However, conventional fabrication techniques rely on cleanroom facilities, which are not easily accessible and are expensive to use, making the overall manufacturing process inconvenient and costly. Moreover, the inherent time-consuming nature of current fabrication procedures impede the rapid customization of neural probes in between *in vivo* studies. Here, we introduce a new technique stemming from 3D printing technology for the low-cost, mass production of rapidly customizable optogenetic neural probes. We detail the 3D printing production process, on-the-fly design versatility, and biocompatibility of 3D printed optogenetic probes as well as their functional capabilities for wireless *in vivo* optogenetics. Successful *in vivo* studies with 3D printed devices highlight the reliability of this easily accessible and flexible manufacturing approach that, with advances in printing technology, can foreshadow its widespread applications in low-cost bioelectronics in the future.

Graphical abstract

Low-cost, rapidly customizable optogenetic probes are developed using economical and readily accessible 3D printing technology. This 3D printing approach allows deployment of batches of custom-designed probes within minutes, without requiring special cleanroom facilities. Experimental characterization and *in vivo* studies involving 3D printed wireless optogenetic probes demonstrate the utility and feasibility of this manufacturing scheme, indicating its potential for use in construction of various bioelectronics.

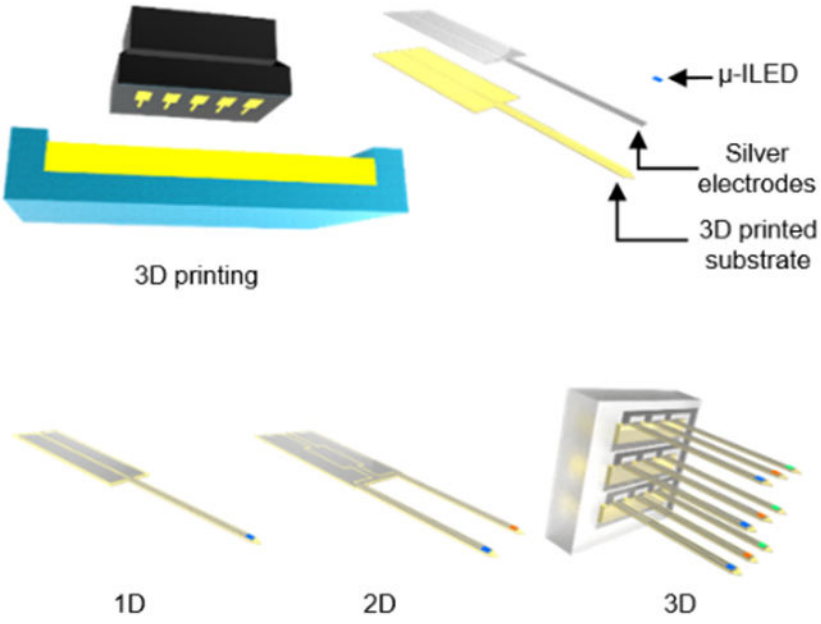

Keywords

3D printing; optogenetics; microfabrication; wireless; neural probe; rapid prototyping

Optogenetics is a highly selective neuromodulation technique that enables cell-type specific manipulation of neural activity using light.[1] Its ability to control neuronal activity with unprecedentedly high spatiotemporal resolution has led to breakthroughs in our understanding of mammalian brain function and neural pathways associated with various neurological, neuropsychological, and neuropathological process.[2,3] Conventionally, implementing optogenetics *in vivo* relies on optical fibers connected to external lasers.[4,5] This approach has been the most commonly used tool for optogenetics since its emergence. Albeit simple and powerful, the optical fiber approach is limited due to its tethered operation and lack of design flexibility, which hinders rapid adaptation to diverse needs for complex neuroscience experiments where the number of light sources, location, depth, and direction of light delivery can be critical variables.

Recent advances in materials and microfabrication techniques have tried to overcome this issue by creating optical neural probes that are customizable in terms of size, dimensions, and functions for minimally invasive versatile operation.[5] This microfabrication-based method not only allows the use of various materials (e.g., silicon,[6–8] SU-8,[9] polyimide (PI),[10,11] polyethylene terephthalate (PET),[12,13] etc.) to build highly biocompatible implants, but also facilitates the direct integration of probes with micron-scale light sources and wireless control units. Together these features enable opportunities for tether-free chronic optogenetics in awake, behaving animals.[10–17] However, this approach requires expensive, bulky equipment and special cleanroom facilities, which make the overall manufacturing costly and limits accessibility to the technology for labs that do not have these equipment or skills. Moreover, modification of a design is time-consuming and

arduous as it requires the need for design of new photomasks and/or development of new fabrication processes. The difficulty in customizability hampers the rapid design adjustment and optimization of neural devices to meet requirements for specific applications. Recent developments have addressed some of these limitations by employing thermal drawing, which does not involve complex cleanroom equipment, for the manufacture of flexible multifunctional fibers.[18] Thermal drawing can, relatively easily, produce polymeric fiber neural probes with different combinations of modalities (e.g., optical, electrical, and fluidic) and various lengths. However, this approach lacks multi-dimensional scalability and still requires access to special equipment and procedures that cannot be easily or rapidly customized. In addition, this fiber-like configuration still relies on tethered operation, which restricts naturalistic behavior during *in vivo* experiments.

Here we report material processes and 3D printing-based fabrication strategies that allow the rapid development of implantable neural probes of any desired design and length. These printing approaches not only eliminate the need for expensive materials, special cleanroom machines, and time-consuming microfabrication procedures, but also provide on-the-fly design customizability. In other words, these probes can be redesigned and deployed for quick turnaround to meet design needs. These probes can be made with minimal skills, equipment, and training, thus significantly reducing the overall cost, time, and effort required for the construction of neural probes for specific target applications. These advances can be particularly useful for the independence of neuroscience laboratories where neuroscientists do not have access to cleanroom resources or skilled training to execute microfabrication to produce neural implants optimized for their needs. Using this unique manufacturing scheme, we deployed various designs of 3D printed optogenetic probes (3D-POPs), which can be assembled with custom-designed wireless control modules. Experimental characterization and successful implementation of wireless *in vivo* optogenetics in mice validate their biocompatibility, reliability, and functionality. The practicality and robustness of this 3D printing approach for facile manufacturing of versatile neural implants demonstrates its utility for experiments in live animals.

Figure 1 presents the highly customizable and rapidly manufacturable nature of 3D-POPs. Mammalian brain research involves animal models of varying sizes, ranging from small rodents to humans, each requiring a different probe design for neuronal interventions at specific tissue locations in the brain as illustrated in Figure 1a. The 3D-POP can be an effective tool in this regard due to its innate ability for easy and quick design adjustment as well as the rapid deployment of optimized structural variations for a wide variety of targeted brain structures in various animal models. Figure 1b highlights the basic architecture of ultrathin (60 μm thick) and minimally-invasive 3D-POPs, which consist of microscale inorganic light-emitting diodes (μ-ILEDs) for optogenetic stimulation, electrodes for μ-ILED control, and a 3D printed substrate for probe construction. The substrate is embedded with superficial micro-grooves (20 μm deep) which enable the uniform and rapid construction of ultrathin electrodes (20.6 ± 2.3 Ω) on the surface (Figure S1, Supporting Information). Their customizability can be further extended to create multi-dimensional configurations (e.g., 2D or 3D) by simple design modification in the 3D printed file.

The key to the facile and swift construction of the probes is 3D printing-based manufacturing. This approach allows versatile scaling and on-the-fly alterations of device design in terms of layouts, lengths and dimensions. Figure 1c and Figure S2 in the Supporting Information present the fabrication process of optogenetic probes using 3D printing. With an appropriate computer-aided design (CAD) file loaded in a 3D printer (B9 Core 530, B9 Creations), the desired shapes and dimensions of probe substrates are printed with a photopolymer (B9R-4-Yellow Resin, B9 Creations) using stereolithography with minimal vertical and lateral resolutions of 20 μm and 30 μm, respectively (step ①). Depending on the size of the build head of the 3D printer, this approach can allow printing of up to 50 distinct probes (total printing area of ~1800 mm^2) in approximately 3 minutes, making it a promising and feasible option for low-cost mass production. After the probes are released from the 3D printer build stage (step ②), silver paste (P-100, CANS) is spread onto the patterned probe substrates with a rubber blade to render the electrodes into the micro-grooves (step ③). Finally, following transfer printing and soldering of μ-ILEDs (220 μm × 270 μm; TR2227, Cree Inc.) at the tips of probes,[19] the probe shanks are coated with a polydimethylsiloxane (PDMS; 1 μm)/parylene C (6 μm) bilayer to provide biocompatibility, chemical inertness, and waterproofing (vapor permeability of parylene C = 0.083 g mm m^{-2} day^{-1})[20] (step ④). Figure 1d–g and Figure S3 in the Supporting Information present fabricated 3D-POPs, highlighting their customizable scalability in dimensions (1D to 3D), length (order of mm to tens of mm), as well as function (photostimulation with various wavelengths of light to activate distinct optogenetic actuators[21]). 3D-POPs can be fabricated as thin as 60 μm, which is comparable to the thickness of a human hair, to enhance their mechanical compliance for biomechanical compatibility with soft brain tissue (Figure 1f and 1g). With this manufacturing scheme, a batch of 3D-POPs with any configuration can be rapidly produced with extremely low cost ($0.54 per probe with 5 mm length; Table S1, Supporting Information) through simple changes in the 3D CAD design. The resulting devices can be powered using both wired (Figure S4, Supporting Information) and wireless schemes (Figure S5–S7, Supporting Information), making them highly versatile and accessible for neuroscience experiments.

Figure 2 shows the electrical, optical, and thermal characteristics of the 3D-POPs. For activation of optogenetic actuators such as channelrhodopsin-2 (ChR2), at least 1 mW mm^{-2} of optical output power is required at a wavelength of ~470 nm light.[1,22] We operated the μ-ILEDs of 3D-POPs with an input voltage of 3 V, and this led to an optical intensity of ~80 mW mm^{-2} (Figure 2a), which is far beyond the minimal threshold for optogenetic stimulation. The probes were able to provide stable and sufficient optical output power even under tight bending, maintaining nearly 80% of performance (~65 mW mm^{-2}) when bent 90° with a radius of curvature of 2 mm, thus demonstrating necessary electromechanical flexibility to enable reliable operation in a dynamic tissue environment and under a curved condition (Figure 2b). For rare applications requiring extremely high flexibility, enhanced electrical stability and reliability could be achieved using elastic conductive composite materials[23–25] instead of the silver paste to build the interconnects of 3D-POPs. Photostimulation using μ-ILEDs is also thermally compatible with neural tissue, therefore ensuring biologically safe operation. To demonstrate this thermal operation with 3D-POPs, we operated the probes in brain tissue (10 ms light pulse width at 5, 10, 20, and 40 Hz) for 2

minutes at each frequency and showed that the temperature increase in brain tissue was < ~1 °C when the μ-ILEDs were operated up to a frequency of 40 Hz with a 10 ms pulse width (Figure 2c). The thermally biocompatible operation of μ-ILEDs has also been confirmed through extensive *in vivo* characterization in several previous studies.[5,10,12–16] Apart from the minimally invasive and biocompatible nature of neural probes, their chronic operational stability in biological fluids is another critical factor to determine their feasibility of use in long-term animal studies. To mimic the biological environment for validation of long-term stability, we immersed 3D-POPs in saline solution (0.9%) at various temperatures (37, 60, and 90 °C) and measured the optical power density of the probes over time to determine how long they could operate without performance degradation by biofluid invasion (Figure 2d). PDMS/parylene C bilayer coating of 3D-POPs served as an excellent barrier against biofluid, thereby helping the 3D-POPs survive for more than 60 days at <90 °C. Theoretical analysis with Arrhenius relation[10] shows that the probes are expected to be operational for a year at physiological temperature (37 °C), which is substantially longer than most neuroscience applications. While parylene C provides robust encapsulation for long-term biological operation, in the case of shorter *in vivo* applications (1-2 months),[15] PDMS alone can be used for probe sealing to simplify the device encapsulation process (Figure S8, Supporting Information).

3D-POPs have bio-favorable mechanical and material properties, which are comparable to those of conventional optical fibers in several aspects. Figure 3a compares the stiffnesses of a 3D-POP and an optical fiber (silica; 200 μm in diameter; FT200EMT, Thorlabs Inc.) with 5 mm length in the physiological frequency range of 0.1–10 Hz. 3D-POPs are 40.6 times less stiff than optical fibers (stiffness at 0.1 Hz: 51.1 N/m for 3D-POPs vs. 2076.6 N/m for optical fibers), yet they are rigid enough to penetrate soft tissue without any external mechanical support. The experiment with phantom brain tissue (0.6% agarose gel) shown in Figure 3b and Video S1 in the Supporting Information verifies that 3D-POPs can be injected into tissue without bending. This was further demonstrated by *in vivo* studies, covered later in this paper, which required precise and accurate implantation of 3D-POPs. This attribute simplifies the surgical process by eliminating the need for injection assist needles,[12–14,17] bioresorbable stiffeners,[16,26,27] or mechanically transformative platforms.[28] When implanted, the probes exert smaller mechanical stress compared to that of an optical fiber on surrounding brain tissue, which continuously vibrates in microscale mainly due to cardiorespiratory functions and locomotion. Figure 3c shows finite element analysis (FEA) results visualizing the maximum principal strains in brain tissue caused by a 3D-POP (left) and an optical fiber (right), assuming 10 μm lateral displacement of tissue by micromotion. The simulation indicates that the strain induced in the surrounding tissue by a 3D-POP is 41% smaller than that caused by an optical fiber due to a large difference in their flexibility. Previous studies have reported a strong relationship between the mechanical strain caused by implanted probes during tissue micromotion and associated inflammation response.[29,30] However, it was not clear whether the 3D printed material is biocompatible and how this variable would affect overall immunoreactive glial responses, a sign of inflammation in the brain. To quantify this inflammatory response, we implanted bare and parylene C-coated 3D-POPs as well as standard 200 μm diameter optical fibers into the dorsal striatum of adult mice[4]. We then examined expression of markers associated with microglia, Iba1 (ionized

calcium binding adaptor molecule 1), and astrocytes, GFAP (glial fibrillary acidic protein), following implantation of optical fibers and 3D-POPs (with and without parylene C coating). Although bare 3D-POPs created significantly larger lesions on average, parylene C coating reduced this response to levels aligned with fiber optic implants, with no significant differences between fiber optic probes and parylene-coated 3D-POPs (Figure 3d–g). Additionally, there were no significant differences across any of the implants in the microglial and astrocytic responses following one month of implantation (Figure 3h–i). These results suggest that parylene C-coated 3D-POPs provide substantially improved biocompatibility. However, parylene C is not perfectly hermetic. Therefore this encapsulation approach would be likely only be suitable for 2-5 years,[31] an operation lifetime far beyond what is typical in laboratory settings.

Figure 4 demonstrates the effectiveness of implementing 3D-POPs for basic behavioral neuroscience experimentation. Here we adapted a well-established behavioral assay in which agouti-related protein (*agrp*) expressing neurons in the arcuate nucleus of the hypothalamus (ARC^{agrp}) are stimulated to drive food consumption in *ad libitum* fed conditions.[32] We implanted 3D-POPs lateral to the paraventricular nucleus of the hypothalamus (PVH) of *agrp*^{Cre} x Ai32 (Cre-dependent ChR2) mice (Figure 4a, d–f) and drove 20 Hz blue light photostimulation within an *ad libitum* feeding assay. Following baseline exposure to a 3 chambered behavioral apparatus, *agrp*^{Cre} x Ai32 mice were given access to chow and sweet pellet diets on 3 consecutive test days (Figure 4b–c). On the second day, blue light was used to photostimulate (20 Hz) ARC^{agrp} afferents within the PVH (ARC^{agrp}-PVH). This activation increased total food intake among PVH-implanted mice compared to off-site (non-PVH) and Cre-negative control mice (Figure 4g–h, Figure S9a–c, Supporting Information). Overall, PVH-implanted mice increased 397 ± 79.6% in baseline consumption during 20 Hz stimulation (Figure 4i). Although mice showed an increase in total food consumption, there were no differences in time spent in environments associated with preferred diets or the preference of specific diets among PVH mice and non-PVH mice (Figure S9d–h, Supporting Information). Overall, these data clearly demonstrate the effectiveness of using 3D-POPs for optogenetic stimulation within behavioral neuroscience experiments.

In summary, the 3D printing approaches reported in this article have immense potential to create a wide variety of low-cost microscale neural probes in a swift manner. This facile, rapid manufacturing technique with on-the-fly design customizability yields biocompatible and functionally robust neural interfacing devices. This straightforward approach can potentially replace neural probes fabricated with standard microfabrication processes involving special and expensive cleanroom facilities. The study presented here focused on the development and *in vivo* validation of 3D printed optogenetic probes for the brain, but the same strategy can be readily applied to produce not only neural probes with other modalities (e.g., electrical, microfluidic, etc.) but also different types of bioelectronic devices optimized for specific needs for various other organs. We envision that the integration of 3D printing manufacturing with advanced materials and packaging schemes will open numerous opportunities for cost-effective, yet powerful wearable and implantable electronics with practical applications in biomedical sciences, healthcare, and medicine.

Experimental section

Design of plug-n-play standalone wireless control modules:

The releasable wireless control module controls the neural probe after decoding the wireless Bluetooth signals sent from the smartphone by the user. It consists of a Bluetooth system-on-chip (RFD77101, RF Digital Corp.), a low-dropout (LDO) regulator (NCP4624, Semiconductor Components Industries LLC), a rechargeable battery (GM300910, PowerStream Holdings Inc.), and a male pin connector (M50-3630342, Harwin Inc.), which are soldered onto a custom-designed flexible printed circuit board (Figure S6, Supporting Information). The Bluetooth chip adjusts the frequency of voltage pulses for μ-ILED operation on-the-fly. The LDO regulator ensures a stable output voltage to the circuit irrespective of the current fluctuations occurring due to different photostimulation frequency requirements. The wireless control module can easily regulate a 3D-POP attached with a female pin connector (M50-3140345, Harwin Inc.) with the simple assembly/disassembly process (Figure S5, S6, and Video S2, Supporting Information). This module allows researchers to optogenetically excite multiple 3D-POPs in the vicinity wirelessly (using a smartphone, Figure S7, Supporting Information), each with a unique stimulation frequency without any line-of-sight handicap, as was seen in several previous studies[12,33]

Mechanical modeling and FEA:

Three dimensional finite element models were established to simulate the mechanical interaction between a neural probe and brain tissue in ABAQUS. The size of the brain tissue was 7 mm × 4 mm × 4 mm. The Young's modulus and Poisson's ratio of the brain were 3.156 kPa and 0.49, respectively.[34] The printed neural probe was 5 mm long, 500 μm wide, and 40 μm thick. Two different material properties were defined for the optical fiber (Young's modulus, E = 68.853 GPa) and 3D printed probe (E = 49.894 GPa). In these models, the interaction type of the probe and surrounding brain tissue was tie contact. Micromotion (10 μm) was simulated by displacing the bottom boundary of the brain tissue while keeping the top edge of the neural probe fixed.

Experimental subjects:

Adult (20 to 30 g) male C57BL/6J and *agrp*-IRES-Cre[35] backcrossed to C57BL/6J mice and bred to Ai32 mice[36] were group-housed, given access to food pellets and water ad libitum, and maintained on a 12-hour:12-hour light:dark cycle (lights on at 6:00 a.m.). All mice were transferred to a facility within the laboratory after weaning and remained in the facility in the laboratory at least 1 week before surgery, after surgery, and throughout the duration of the behavioral assays to minimize stress from transportation and disruption from foot traffic. All procedures were approved by the Animal Care and Use Committee of Washington University (20170202) and conformed to U.S. National Institutes of Health (NIH) guidelines.

Stereotaxic surgery:

3D-POP devices were implanted as previously described[28] with minor modifications to accommodate the 3D-POP probe. Briefly, after the mice were acclimatized to the holding

facility for 7 to 21 days, they were anaesthetized in an induction chamber (4% isoflurane) and placed in a stereotaxic frame (model 942, KopfInstruments), where they were maintained at 1 to 2% isoflurane. A standard cannula holder (model 1776-P1, KopfInstruments) was adapted to implant the 3D-POPs. Devices were ethanol-sterilized before the implantation and secured with C&B Metabond (Parkell). For the glial response studies, mice were implanted with 3D-POPs in the dorsal striatum [stereotaxic coordinates from bregma: anterior-posterior (AP), +1.10 mm; medial-lateral (ML), ±1.50 mm; dorsal-ventral (DV), −4.00 mm]. For the optogenetic feeding experiment, *agrp*-IRES-Cre × Ai32 mice were implanted with the 3D-POP adjacent to the PVH (stereotaxic coordinates from bregma: AP, −0.82 mm; ML, −0.5 mm; DV, −5.25 mm). Further, two subsets of animals were used as distinct control groups: 1) Cre negative animals implanted in the PVH, 2) Cre positive animals implanted in the dorsal striatum (as described above). Following blinded histological confirmation, all dorsal striatum and off-target implanted $agrp^{Cre}$ mice were designated as non-PVH for all analyses. Mice were allowed to recover 1 week following implantation before behavioral testing.

Immunohistochemistry:

Immunohistochemistry was performed as described.[28] Briefly, mice were anesthetized with a ketamine/xylazine/acepromazine cocktail and intracardially perfused with paraformaldehyde in phosphate-buffered saline (PBS). Brains were dissected, postfixed for 24 hours at 4°C, cryoprotected with solution of 30% sucrose in 0.1 M phosphate buffer (PB) at 4°C for at least 24 hours, cut into 35-μm sections, and processed for immunostaining. Brain sections (35 μm) were washed three times in PBS and blocked in PBS containing 0.5% Triton X-100 and 5% normal goat serum. For glial responses in implanted tissues, horizontal sections were then incubated for ~16 hours at room temperature in guinea pig anti-GFAP (glial fibrillary acidic protein) (1:500; Synaptic Systems) and rabbit anti-Iba1 (1:300; Wako Chemicals). Following incubation, sections were washed three times in PBS and incubated for 2 hours at room temperature in Alexa Fluor 488 goat anti-rabbit immunoglobulin G (1:1000; Invitrogen) and goat anti–guinea pig Alexa Fluor 546 (1:1000; Invitrogen), washed three times in PBS and incubated for 1 hour in NeuroTrace 435/455 Blue Fluorescent Nissl stain (1:400), and then washed three times in PBS, followed by three 10-min washes in PB, and mounted on glass slides with HardSet Vectashield (Vector Laboratories). For tissue from the feeding studies, sections were washed three times in PBS, followed by three 10-min washes in PB, and mounted on glass slides with HardSet Vectashield with 4′,6-diamidino-2-phenylindole (DAPI) (Vector Laboratories). All sections were imaged on an epifluorescent microscope, and z-stacks were taken throughout the focal plane. 3D deconvolution was then performed, and images are presented as a maximum projection of that 3D deconvolution. Gain and exposure time were constant throughout each experiment, and all image groups were processed in parallel and analyzed using ImageJ (NIH).

Food consumption assay:

The food intake study was performed at the onset of the light cycle to increase probability of baseline satiety. All animals were singly housed for at least 2 weeks following surgery and handled daily to ensure acclimation and minimize any stress response to experimental

procedures. We used a modified three-chamber apparatus consisting of two square boxes (27 cm × 27 cm) that served as the food chambers separated by a small center area that served as the passageway (5 cm wide × 8 cm long) between boxes. Boxes had 2.5 cm black-and-white vertical stripes or horizontal stripes and a small weigh boat fixed to the chamber floor. Mice were handled each day for 1 week and given 1 gram of each test diet for 3 consecutive days prior to behavioral testing to reduce neophobia. The behavioral testing was completed over 5 consecutive days. On each test day, each mouse was briefly handled to be connected to a battery-powered BLE device, and placed into the apparatus. On day zero of testing, mice were allowed to explore all three regions of the box with no food present for 1 hour. On day one, sweetened and chow pellet diets were placed in opposite chambers of the apparatus. Mice were allowed to explore the apparatus and freely consume each diet for 1 hour. On day two, mice received blue μ-ILED photostimulation at 20 Hz immediately prior to the placement into the apparatus and continuously for the entirety of the test. Mice were allowed to explore the apparatus and consume each diet for 1 hour. On day three, sweetened and chow pellet diets were placed in opposite chambers and mice were allowed to explore the apparatus and freely consume each diet for 1 hour, with no stimulation. On day four, mice were allowed to explore all three regions of the box with no food present for 1 hour. The weight of each diet was measured before and after each test. Locomotor and position data were monitored with EthoVision 11.0 (Noldus). Preference scores were calculated with regard to the side in which each mouse consumed the most food during 20 Hz stimulation on day two (Preferred food-side). The calculation subtracted the time spent on the Preferred food-side during day zero from time spent in this side during day four testing. Mice with implantation outside the PVH expression were excluded from the group after blind histological examination by a separate experimenter and added here to the non-PVH group. By this process, all food intake measurements were randomized and blind to the experimenter.

Diets:

The diets used for this experimentation were 20 mg, Dustless Precision Pellets® available from Bio-Serv (Flemington, NJ). The chow diet (Product #0163) was 3.35 kcal/g and consisted of 21.3% protein, 3.8% fat, and 54% carbohydrate. The sweetened diet (Product #F0071) was 3.6 kcal/g and consisted of 18.7% protein, 5.6% fat, and 59.1% carbohydrate.

Supplementary Material

Refer to Web version on PubMed Central for supplementary material.

Acknowledgements

We thank Prof. Daesoo Kim’s lab at KAIST for explanted tissue. This paper is based on a research which has been conducted as part of the KAIST-funded Global Singularity Research Program for 2020. This work was also supported by the National Research Foundation of Korea (grant nos. NRF-2018R1C1B6001706 and NRF-2017M3A9G8084463, J.-W.J.), the Brain & Behavior Research Foundation (J.G.M.), and the United States National Institutes of Health (R25MH112473, J.B.).

References

[1]. Yizhar O, Fenno LE, Davidson TJ, Mogri M, Deisseroth K, Neuron 2011, 71, 9. [PubMed: 21745635]

[2]. Tye KM, Deisseroth K, Nat. Rev. Neurosci 2012, 13, 251. [PubMed: 22430017]

[3]. Inoue K, Takada M, Matsumoto M, Nat. Commun 2015, 6, 8378. [PubMed: 26387804]

[4]. Sparta DR, Stamatakis AM, Phillips JL, Hovelsø N, van Zessen R, Stuber GD, Nat. Protoc 2012, 7, 12.

[5]. Qazi R, Kim CY, Byun S-H, Jeong J-W, Front. Neurosci 2018, 12, 764. [PubMed: 30405343]

[6]. Scharf R, Tsunematsu T, McAlinden N, Dawson MD, Sakata S, Mathieson K, Sci. Rep 2016, 6. [PubMed: 28442741]

[7]. Shin H, Son Y, Chae U, Kim J, Choi N, Lee HJ, Woo J, Cho Y, Yang SH, Lee CJ, Cho I-J, Nat. Commun 2019, 10, 3777. [PubMed: 31439845]

[8]. Kampasi K, English DF, Seymour J, Stark E, McKenzie S, Vöröslakos M, Buzsáki G, Wise KD, Yoon E, Microsyst. Nanoeng 2018, 4, 10. [PubMed: 30766759]

[9]. Fan Bin, Kwon Ki Yong, Weber AJ, Wen Li, In 2014 36th Annual International Conference of the IEEE Engineering in Medicine and Biology Society; IEEE: Chicago, IL, 2014; pp. 450–453.

[10]. Shin G, Gomez AM, Al-Hasani R, Jeong YR, Kim J, Xie Z, Banks A, Lee SM, Han SY, Yoo CJ, Lee J-L, Lee SH, Kurniawan J, Tureb J, Guo Z, Yoon J, Park S-I, Bang SY, Nam Y, Walicki MC, Samineni VK, Mickle AD, Lee K, Heo SY, McCall JG, Pan T, Wang L, Feng X, Kim T, Kim JK, Li Y, Huang Y, Gereau RW, Ha JS, Bruchas MR, Rogers JA, Neuron 2017, 93, 509. [PubMed: 28132830]

[11]. Samineni VK, Yoon J, Crawford KE, Jeong YR, McKenzie KC, Shin G, Xie Z, Sundaram SS, Li Y, Yang MY, Kim J, Wu D, Xue Y, Feng X, Huang Y, Mickle AD, Banks A, Ha JS, Golden JP, Rogers JA, Gereau RW, PAIN 2017, 158, 2108. [PubMed: 28700536]

[12]. Qazi R, Gomez AM, Castro DC, Zou Z, Sim JY, Xiong Y, Abdo J, Kim CY, Anderson A, Lohner F, Byun S-H, Chul Lee B, Jang K-I, Xiao J, Bruchas MR, Jeong J-W, Nat. Biomed. Eng 2019, 3, 655. [PubMed: 31384010]

[13]. Jeong J-W, McCall JG, Shin G, Zhang Y, Al-Hasani R, Kim M, Li S, Sim JY, Jang K-I, Shi Y, Hong DY, Liu Y, Schmitz GP, Xia L, He Z, Gamble P, Ray WZ, Huang Y, Bruchas MR, Rogers JA, Cell 2015, 162, 662. [PubMed: 26189679]

[14]. Kim T.-i., McCall JG, Jung YH, Huang X, Siuda ER, Li Y, Song J, Song YM, Pao HA, Kim R-H, Lu C, Lee SD, Song I-S, Shin G, Al-Hasani R, Kim S, Tan MP, Huang Y, Omenetto FG, Rogers JA, Bruchas MR, Science 2013, 340, 211. [PubMed: 23580530]

[15]. Park SI, Brenner DS, Shin G, Morgan CD, Copits BA, Chung HU, Pullen MY, Noh KN, Davidson S, Oh SJ, Yoon J, Jang K-I, Samineni VK, Norman M, Grajales-Reyes JG, Vogt SK, Sundaram SS, Wilson KM, Ha JS, Xu R, Pan T, Kim T, Huang Y, Montana MC, Golden JP, Bruchas MR, Gereau RW, Rogers JA, Nat. Biotechnol 2015, 33, 1280. [PubMed: 26551059]

[16]. Noh KN, Park SI, Qazi R, Zou Z, Mickle AD, Grajales-Reyes JG, Jang K-I, Gereau RW, Xiao J, Rogers JA, Jeong J-W, Small 2018, 14, 1702479.

[17]. McCall JG, Qazi R, Shin G, Li S, Ikram MH, Jang K-I, Liu Y, Al-Hasani R, Bruchas MR, Jeong J-W, Rogers JA, Nat. Protoc 2017, 12, 219. [PubMed: 28055036]

[18]. Canales A, Jia X, Froriep UP, Koppes RA, Tringides CM, Selvidge J, Lu C, Hou C, Wei L, Fink Y, Anikeeva P, Nat. Biotechnol 2015, 33, 277. [PubMed: 25599177]

[19]. McCall JG, Kim T, Shin G, Huang X, Jung YH, Al-Hasani R, Omenetto FG, Bruchas MR, Rogers JA, Nat. Protoc 2013, 8, 2413. [PubMed: 24202555]

[20]. Massey LK, Permeability Properties of Plastics and Elastomers: a Guide to Packaging and Barrier Materials.; 2003.

[21]. Klapoetke NC, Murata Y, Kim SS, Pulver SR, Birdsey-Benson A, Cho YK, Morimoto TK, Chuong AS, Carpenter EJ, Tian Z, Wang J, Xie Y, Yan Z, Zhang Y, Chow BY, Surek B, Melkonian M, Jayaraman V, Constantine-Paton M, Wong GK-S, Boyden ES, Nat. Methods 2014, 11, 338. [PubMed: 24509633]

[22]. Deng W, Goldys EM, Farnham MM, Pilowsky PM, Am. J. Physiol.-Regul. Integr. Comp. Physiol 2014, 307, R1292. [PubMed: 25274906]

[23]. Li Z, Le T, Wu Z, Yao Y, Li L, Tentzeris M, Moon K-S, Wong CP, Adv. Funct. Mater 2015, 25, 464.

[24]. Kisannagar RR, Jha P, Navalkar A, Maji SK, Gupta D, ACS Omega 2020, 5, 10260. [PubMed: 32426582]

[25]. Santhiago M, Corrêa CC, Bernardes JS, Pereira MP, Oliveira LJM, Strauss M, Bufon CCB, ACS Appl. Mater. Interfaces 2017, 9, 24365. [PubMed: 28650141]

[26]. Guan S, Wang J, Gu X, Zhao Y, Hou R, Fan H, Zou L, Gao L, Du M, Li C, Fang Y, Sci. Adv 2019, 5, eaav2842. [PubMed: 30944856]

[27]. Jeon M, Cho J, Kim YK, Jung D, Yoon E-S, Shin S, Cho I-J, J. Micromechanics Microengineering 2014, 24, 025010.

[28]. Byun S-H, Sim JY, Zhou Z, Lee J, Qazi R, Walicki MC, Parker KE, Haney MP, Choi SH, Shon A, Gereau GB, Bilbily J, Li S, Liu Y, Yeo W-H, McCall JG, Xiao J, Jeong J-W, Sci. Adv 2019, 5, eaay0418. [PubMed: 31701008]

[29]. Nguyen JK, Park DJ, Skousen JL, Hess-Dunning AE, Tyler DJ, Rowan SJ, Weder C, Capadona JR, J. Neural Eng 2014, 11, 056014. [PubMed: 25125443]

[30]. Sridharan A, Nguyen JK, Capadona JR, Muthuswamy J, J. Neural Eng 2015, 12, 036002. [PubMed: 25834105]

[31]. Implantable biomedical microsystems: design principles and applications; Bhunia S; Majerus SJ; Sawan M, Eds.; Micro & nano technologies series; Elsevier/WA, William Andrew is an imprint of Elsevier: Amsterdam ; Boston, 2015.

[32]. Atasoy D, Betley JN, Su HH, Sternson SM, Nature 2012, 488, 172. [PubMed: 22801496]

[33]. Kawakami C, Qazi R, Kim CY, Takahashi K, Jeong J-W, In 2019 International Conference on Optical MEMS and Nanophotonics (OMN); IEEE: Daejeon, Korea (South), 2019; pp. 6–7.

[34]. Hamzavi N, Tsang WM, Shim VPW, In 2013 6th International IEEE/EMBS Conference on Neural Engineering (NER); IEEE: San Diego, CA, USA, 2013; pp. 1119–1122.

[35]. Tong Q, Ye C-P, Jones JE, Elmquist JK, Lowell BB, Nat. Neurosci 2008, 11, 998. [PubMed: 19160495]

[36]. Madisen L, Mao T, Koch H, Zhuo J, Berenyi A, Fujisawa S, Hsu Y-WA, Garcia AJ, Gu X, Zanella S, Kidney J, Gu H, Mao Y, Hooks BM, Boyden ES, Buzsáki G, Ramirez JM, Jones AR, Svoboda K, Han X, Turner EE, Zeng H, Nat. Neurosci 2012, 15, 793. [PubMed: 22446880]

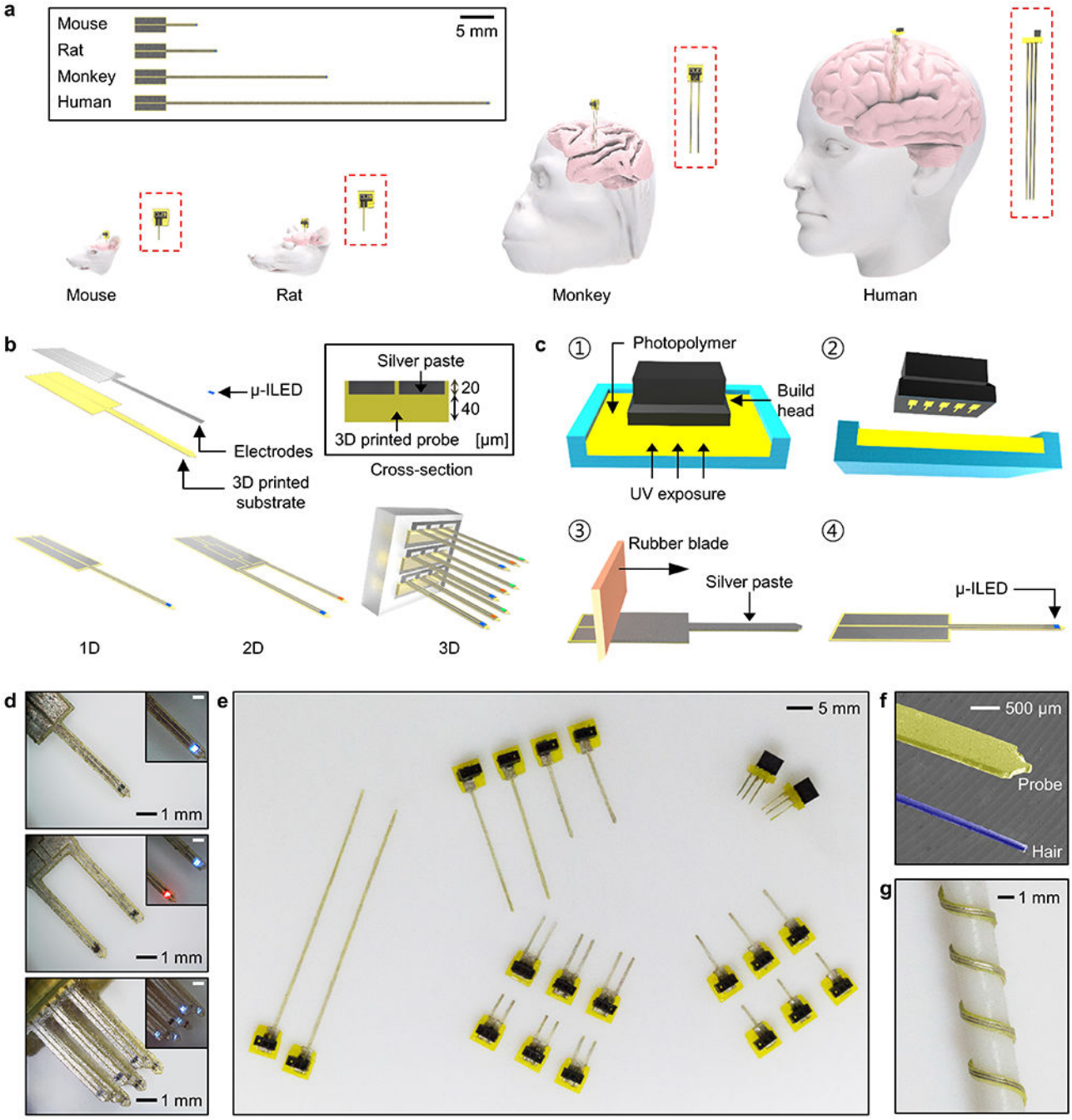

Figure 1.

Concept and design of low-cost and rapidly customizable 3D printed optogenetic probes (3D-POPs). a) Schematic illustration of 3D-POPs highlighting their customizable scalability in terms of length and dimension for applications involving various mammalian brains with different sizes. Insets show magnified view of each probe implanted in a corresponding animal brain. b) Exploded view illustration of the 3D-POP illustrating its basic architecture and design variations for 1D, 2D, and 3D configurations, which can be rapidly manufactured by 3D printing. The inset shows the cross-section of a probe. c) Illustration of the fabrication

steps of a 3D-POP: (1) print desired probes using stereolithography, (2) carefully remove the printed probes and wash them to remove excess residue, (3) apply silver paste over the microgroove surface of the probes and traverse the surface longitudinally with a rubber blade, and (4) attach a microscale inorganic light-emitting diode (μ-ILED) at the probe tip. d) Optical images of 1D (top), 2D (middle), and 3D (bottom) constructions of 3D-POPs, demonstrating simple yet versatile customizability in structural design. μ-ILEDs with desired colors (e.g., blue, red, green, etc.) can be integrated onto probe tips for specific application needs (inset; scale bars, 500 μm). e) Optical image of 3D-POPs with diverse lengths and dimensions fabricated by rapid serial 3D printing. Fifty 5 mm long probes can be printed within 3 minutes. f) Scanning electron micrograph comparing thicknesses of a 3D-POP (yellow) and a human hair (blue). g) Optical image of a 3D-POP wound around a rod (1.5 mm in radius), demonstrating its flexibility.

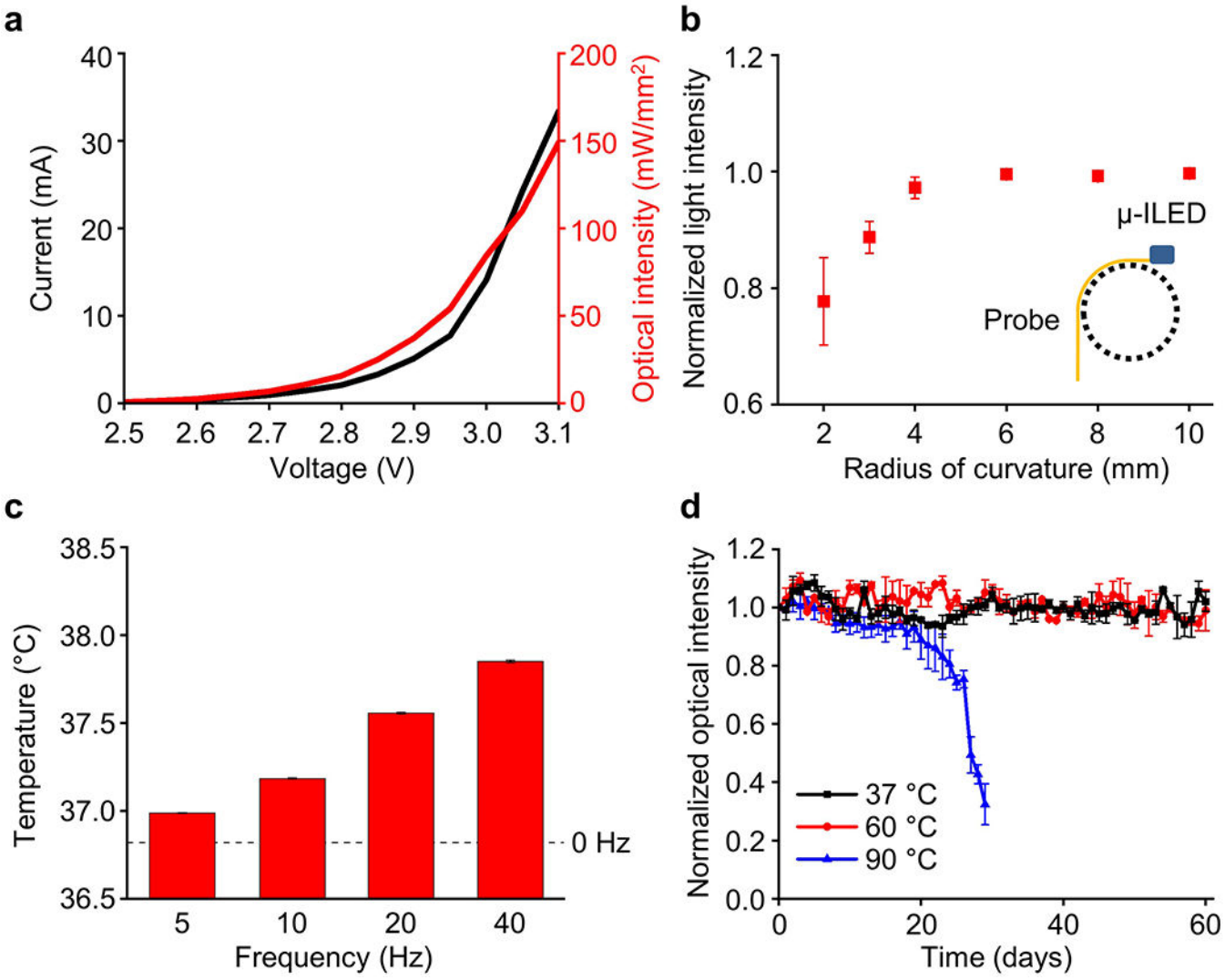

Figure 2.

Electrical, optical, and thermal characteristics of 3D-POPs. a) Current and optical intensity of μ-ILEDs as a function of supplied voltage. b) Normalized light intensity of μ-ILEDs for 3D-POPs bent at 90° with a radius of curvature ranging from 2 to 10 mm. c) Temperature change in brain tissue during the μ-ILED operation at different pulse frequencies (5, 10, 20, and 40 Hz; 10 ms pulse width), measured using an infrared camera after insertion of a μ-ILED into brain tissue at a depth of 1 mm. d) Normalized optical intensity of 3D-POPs as a function of time in saline water (0.9%) at physiological and extreme temperatures (37, 60, and 90 °C).

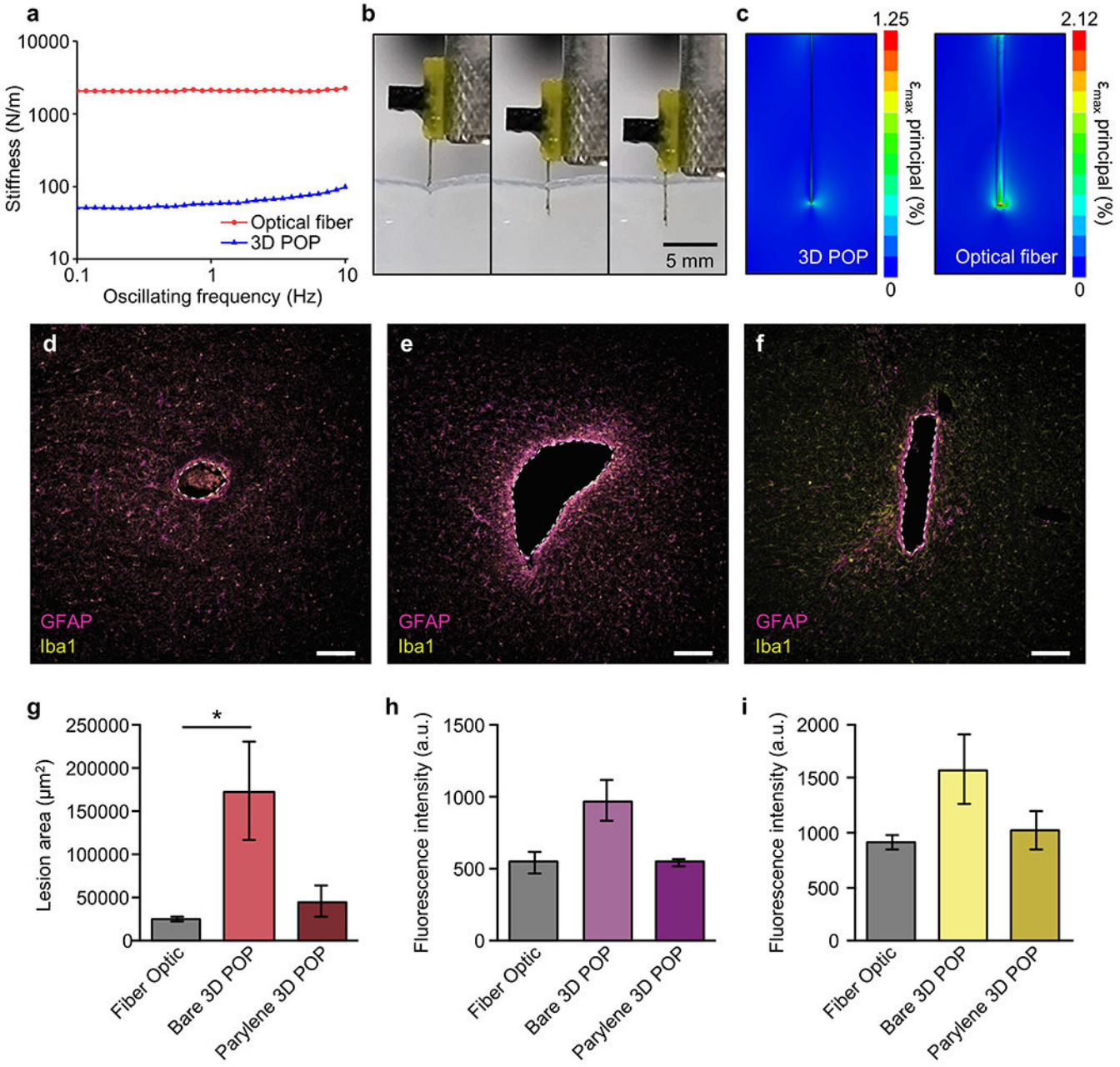

Figure 3.

Mechanical characteristics of 3D-POPs and their biomechanical interaction with brain tissue. a) Plot comparing stiffnesses of 5 mm long 3D-POPs and optical fibers (200 μm in diameter) at physiological frequency (0.1–10 Hz). b) Sequence of optical images showing implantation of a 3D-POP into phantom brain tissue (0.6% agarose gel) without bending. c) FEA simulation visualizing mechanical stress induced in brain tissue by a 3D-POP (left) and an optical fiber (right) due to tissue micromotions (amplitude of micromotion = 10 μm). d-f) Representative immunofluorescence images of 30 μm horizontal slices of brain tissue depicting immune response to implantation. Tissue stained for astrocytes [glial fibrillary acidic protein (GFAP), purple] and activated microglia (Iba1, yellow) from 200μm fiber

optic (d), bare 3D-POP (e), and parylene C-coated 3D-POP (f) neural probes. Scale bars, 50 μm. g) Average lesion area (μm^2) in tissue following implantation of fiber optic (n = 11), bare 3D-POP (n = 10), and parylene C-coated 3D-POP (n = 8) neural probes. A nested one-way ANOVA revealed a significant difference in lesion area, $F(2, 7) = 6.64$, $p < 0.05$). Tukey's multiple comparisons test showed a significant difference in lesion area between fiber optic and bare 3D-POPs ($p < 0.05$), but no significant difference in lesion area for parylene C-coated 3D-POPs compared to fiber optic ($p = 0.77$) or bare 3D-POPs ($p = 0.08$). h-i) Average fluorescence intensity of GFAP (h) and Iba1 (i) expression in tissue following implantation of fiber optic (n = 10), bare 3D-POP (n = 16), and parylene C-coated 3D-POP (n = 8) neural probes (data are mean ± SEM, a.u., arbitrary units). Nested one-way ANOVAs did not reveal any significant difference in GFAP expression, ($F(2, 8) = 2.52$, $p = 0.14$), nor Iba1 expression ($F(2, 8) = 0.53$, $p = 0.61$).

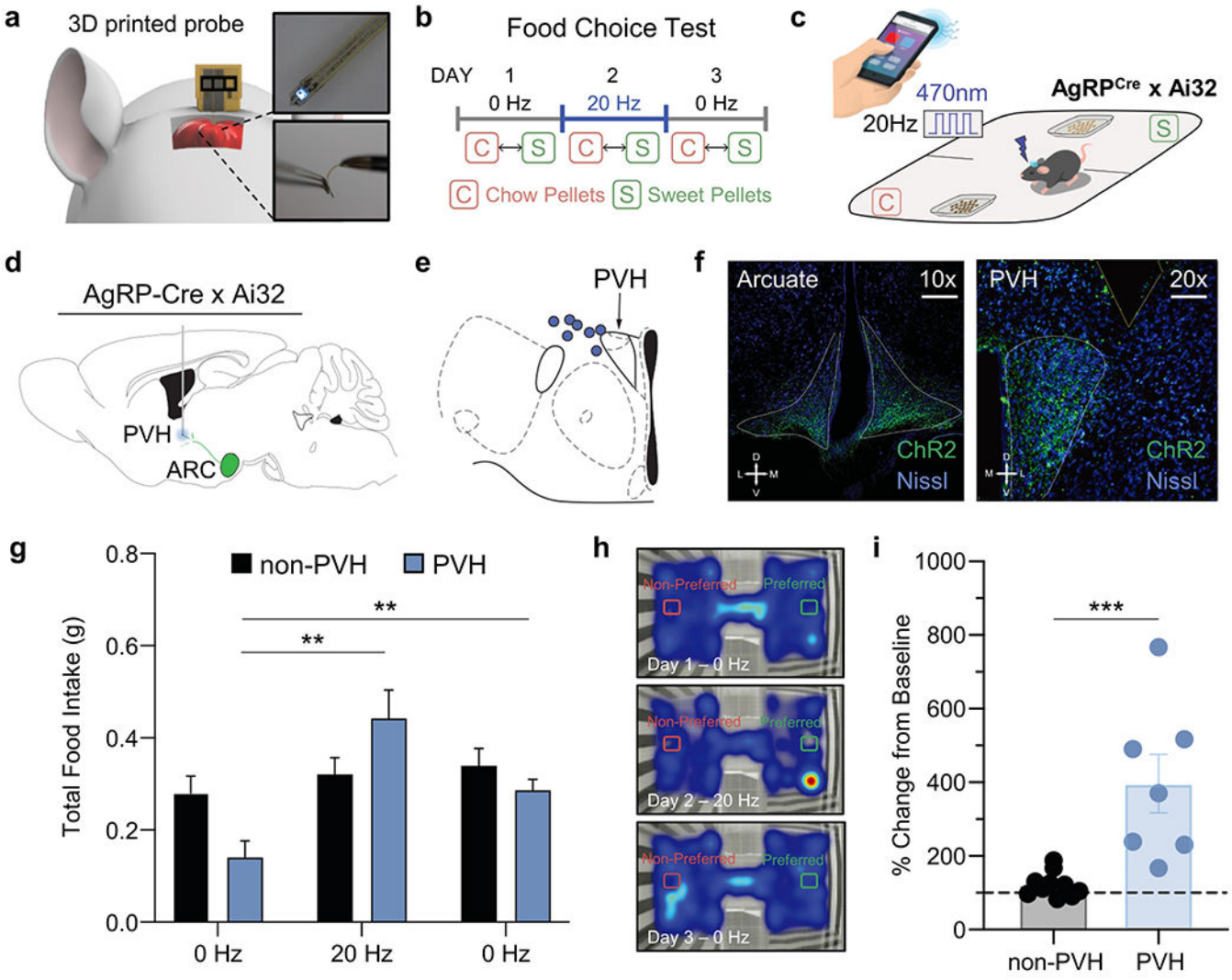

Figure 4.

In vivo behavioral experimentation using 3D-POPs. a) Cartoon diagram depicting intracranial placement of probe, inset: photographs of probe. b) Diary of food choice test depicting timeline for optogenetic stimulation. c) Cartoon schematic of food choice test and stimulation control. d) Representative atlas cartoon depicting placement of 3D-POPs into the paraventricular nucleus of the hypothalamus (PVH) of channelrhodopsin-expressing AgRP-Cre x Ai32 (ChR2-eYFP) mice. e) Atlas cartoon showing correct targeting of the PVH (blue circles indicate confirmed correct placement of 3D-POP. f) Representative coronal immunohistological images of the arcuate nucleus (left panel) and PVH (right panel) depicting expressing ChR2 in *agrp*^{Cre}. Images show ChR2 (green) and Nissl (blue). Scale bars indicate 200 μm and 100 μm, respectively. g) Graph depicting total food consumed over 1 hour during 0 Hz and 20 Hz stimulation in PVH mice compared to non-PVH mice (Mixed-effects model analysis, Group x Stimulation, $F(2, 30) = 17.11$, $p < 0.001$. Tukey's multiple comparisons revealed 20 Hz stimulation increases food consumption in PVH mice compared to 0 Hz stimulations, ** $p < 0.01$). h) Representative heatmaps depicting cumulative time spent with Preferred and Non-Preferred diets for PVH stimulation on Days

1-3. i) Graph depicting the percentage change in total food consumption during 20 Hz stimulation from baseline consumption (0 Hz) for non-PVH and PVH implanted mice (Student's t-test, $t = 4.116$, $n = 17$, *** indicates $p < 0.001$).